

Fermi-Surface Topology and Pairing Symmetry in BiS₂-Based Layered Superconductors

Tomoaki Agatsuma, Takashi Hotta*

Department of Physics, Tokyo Metropolitan University, 1-1 Minami-Osawa, Hachioji, Tokyo 192-0397, Japan

arXiv:1507.05400v1 [cond-mat.supr-con] 20 Jul 2015

Abstract

In order to clarify superconducting properties of BiS₂-based layered superconductors LaO_{1-x}F_xBiS₂, we evaluate the superconducting transition temperature T_c and analyze the gap function in a weak-coupling limit on the basis of the two-dimensional two-orbital Hubbard model. It is found that T_c becomes maximum at $x = 0.6$ in the present calculations. For $x < 0.45$, we obtain the d -wave gap of which line nodes do not cross the pocket-like Fermi-surface curves with the centers at X and Y points. On the other hand, for $x > 0.45$, the extended s -wave gap is found for a couple of large Fermi-surface curves with the centers at M and X points. The variation of the Fermi-surface topology plays a key role for the gap symmetry in BiS₂-based superconductors.

Keywords: BiS₂, Fermi surface, superconductivity, extended s -wave, d -wave

1. Introduction

Since the discovery of new BiS₂-based layered superconductors LaO_{1-x}F_xBiS₂ by Mizuguchi *et al.* [1, 2, 3], both experimental and theoretical investigations for the normal and superconducting properties on BiS₂-based materials have been performed intensively. This material group has the characteristic layered structure, similar to high- T_c cuprate superconductors, where T_c denotes the superconducting transition temperature. Namely, BiS₂ superconducting layer is sandwiched by insulating block layers.

Among several BiS₂-based compounds, first we pick up the mother compound LaOBiS₂. This material is insulating, but by substituting F for O, we can dope electrons into the BiS₂ layer. Then, the system becomes metallic and at low temperatures, superconductivity occurs eventually. In particular, at $x = 0.5$, the superconducting transition temperature T_c becomes maximum [3]. The highest T_c among BiS₂ material groups has been obtained in the sample synthesized under high pressures [4]. It has been reported that the onset T_c is 11.1 K and the temperature at which the resistivity becomes zero is 8.5 K.

Although the mechanism of superconductivity in BiS₂-based materials has not been confirmed yet, the canonical model for this system has been proposed by Usui *et al.* [5, 6], just after the discovery of BiS₂-based superconductors. The minimal model to describe electronic structure of BiS₂ layer is the two-band Hamiltonian composed of Bi $6p_x$ and $6p_y$ orbitals on the two-dimensional square lattice. The appearance of superconductivity has been discussed from various theoretical viewpoints on the basis of this two-orbital Hubbard model [7, 8, 9, 10, 11]. The effects of electron-phonon interaction [12, 13, 14] and spin-orbit coupling [15] have been also discussed. The relation between the characteristic change of the Fermi-surface topology

and the symmetry of the superconducting gap function have been pointed out in previous works [5, 6, 7, 8, 9, 10].

Concerning the gap symmetry, some theoretical studies suggested that the gap function in BiS₂-based layered superconductors could be explained by extended s -wave, d -wave, triplet or other unconventional pairing scenarios [5, 7, 8, 9, 10, 11]. On the other hand, s -wave pairing due to electron-phonon interaction has been also discussed [12, 13, 14]. From experimental viewpoints, the results consistent with s - or extended s -wave pairing have been found in the temperature dependence of the superfluid density in Bi₄O₄S₃ [16], LaO_{0.5}F_{0.5}BiS₂ [17], and NdO_{1-x}F_xBiS₂ [18]. In particular, for NdO_{1-x}F_xBiS₂, it has been reported that the gap symmetry is consistent with s - or extended s -wave both for $x = 0.3$ and 0.5 [18]. It is interesting to consider a way to reconcile those results on the symmetry of the gap function from a viewpoint of Fermi-surface topology characteristic to multi-band systems.

In this paper, we analyze the two-dimensional two-band model including intra- and inter-orbital Coulomb interactions within a random phase approximation (RPA) to derive the effective pairing interaction to induce the Cooper pair. Then, we solve the gap equation to obtain T_c and analyze the gap symmetry by focusing on the Fermi-surface topology. For $x = 0.3$ and 0.4 , we obtain the d -wave gap, but the disconnected Fermi-surface curves with the centers at X and Y points do *not* cross the line nodes of the d -wave gap. When we increase x , we observe the elevation of T_c except for a narrow region around at $x = 0.45$ and the conversion of the gap symmetry from d -wave to extended s -wave. In fact, T_c takes the maximum value at $x = 0.6$. For $x = 0.5$ and 0.6 , we obtain the extended s -wave gap for a couple of large Fermi-surface curves with the centers at Γ and M points. It is proposed that the conversion of the gap symmetry is characteristically induced by the variation of the Fermi-surface topology in the BiS₂-layered materials. Throughout this paper, we use such units as $\hbar = k_B = 1$.

*Corresponding author

Email address: hotta@tmu.ac.jp (Takashi Hotta)

2. Model and Formulation

2.1. Model Hamiltonian

The model Hamiltonian is given by [5, 6]

$$\begin{aligned}
H = & \sum_{k\sigma\tau\tau'} \varepsilon_{k\tau\tau'} c_{k\tau\sigma}^\dagger c_{k\tau'\sigma} + U \sum_{i\tau} n_{i\tau\uparrow} n_{i\tau\downarrow} \\
& + U' \sum_i n_{i1} n_{i2} + J \sum_{i,\sigma,\sigma'} c_{i1\sigma}^\dagger c_{i2\sigma'}^\dagger c_{i1\sigma'} c_{i2\sigma} \\
& + J' \sum_{1,\tau\neq\tau'} c_{i\tau\uparrow}^\dagger c_{i\tau\downarrow}^\dagger c_{i\tau'\downarrow} c_{i\tau'\uparrow},
\end{aligned} \quad (1)$$

where $c_{k\mu\sigma}$ is the annihilation operator of electron with wave-vector \mathbf{k} and spin σ in the orbital τ ($=1$ and 2), $\varepsilon_{k\tau\tau'}$ is the electron energy between τ and τ' orbitals, $n_{i\tau\sigma} = c_{i\tau\sigma}^\dagger c_{i\tau\sigma}$, $n_{i\tau} = \sum_{\sigma} n_{i\tau\sigma}$, and the coupling constants U , U' , J , and J' denote the intra-orbital Coulomb, inter-orbital Coulomb, exchange, and pair-hopping interactions, respectively. Note the relations of $U = U' + J + J'$ and $J = J'$.

2.2. Electron dispersion

As for the electron dispersion relation, by following the results in the paper of Usui *et al.*[5], we obtain

$$\begin{aligned}
\varepsilon_{k11} = & t_0 + 2t_1(\cos k_x + \cos k_y) \\
& + 2t_3 \cos(k_x - k_y) + 2t_4 \cos(k_x + k_y) \\
& + 2t_6[\cos(2k_x + k_y) + \cos(k_x + 2k_y)] \\
& + 2t_8[\cos(2k_x - k_y) + \cos(k_x - 2k_y)],
\end{aligned} \quad (2)$$

$$\begin{aligned}
\varepsilon_{k22} = & t_0 + 2t_1(\cos k_x + \cos k_y) \\
& + 2t_3 \cos(k_x + k_y) + 2t_4 \cos(k_x - k_y) \\
& + 2t_6[\cos(2k_x - k_y) + \cos(k_x - 2k_y)] \\
& + 2t_8[\cos(2k_x + k_y) + \cos(k_x + 2k_y)],
\end{aligned} \quad (3)$$

and

$$\begin{aligned}
\varepsilon_{k12} = & \varepsilon_{k21} \\
= & 2t_2(\cos k_x - \cos k_y) + 2t_5(\cos 2k_x - \cos 2k_y) \\
& + 4t_7(\cos 2k_x \cos k_y - \cos k_x \cos 2k_y).
\end{aligned} \quad (4)$$

The values of $t_0 \sim t_8$ are given by $t_0=2.811$, $t_1=-0.167$, $t_2=0.107$, $t_3=0.880$, $t_4=0.094$, $t_5=-0.028$, $t_6=0.014$, $t_7=0.020$, and $t_8=0.069$ in the unit of eV [5].

The band dispersion is given by

$$E_{k\pm} = \frac{1}{2} \left[\varepsilon_{k11} + \varepsilon_{k22} \pm \sqrt{(\varepsilon_{k11} - \varepsilon_{k22})^2 + \varepsilon_{k12}^2} \right]. \quad (5)$$

Hereafter we define $E_{k+} = E_{kA}$ and $E_{k-} = E_{kB}$, which are called the A and B bands, respectively.

The band structure has been discussed in Ref. [5], but in order to make this paper self-contained, we show E_{kA} and E_{kB} along the path with high symmetry on the Brillouin zone in Fig. 1(a). For $x = 0.3$ and 0.4 , as shown in the insets, we observe that the Fermi levels cross only the B band near the X point, while between M and Γ points, they do not cross the band B. For $x = 0.5$, the Fermi level turns to cross the band B between M

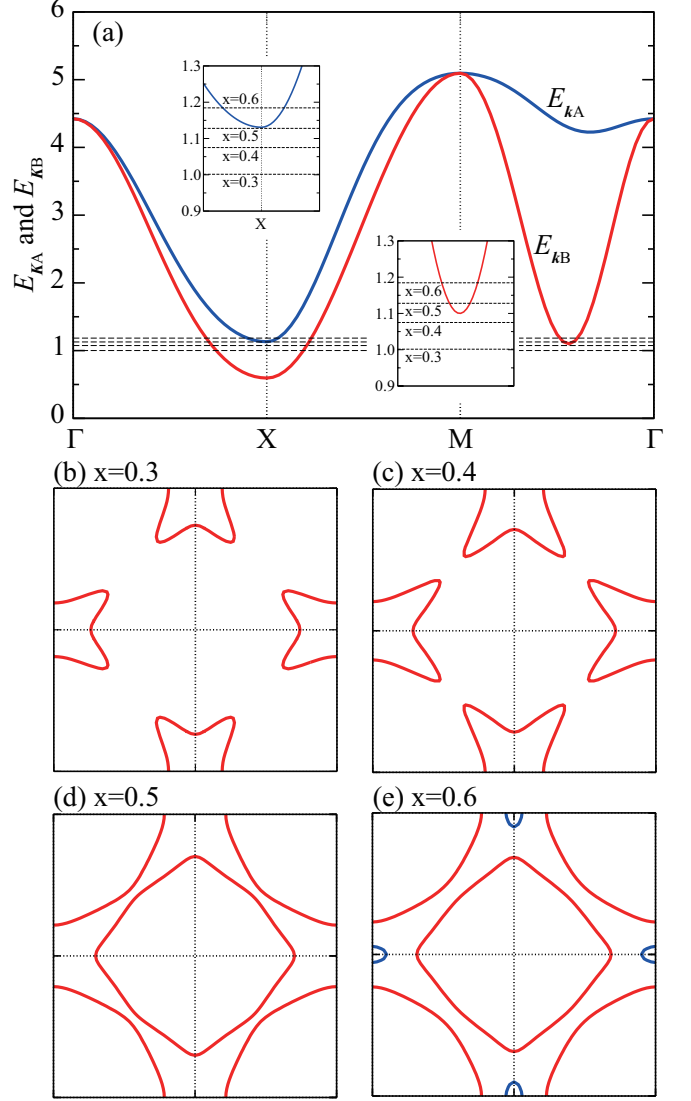


Figure 1: (a) E_{kA} and E_{kB} along the path of $\Gamma \rightarrow X \rightarrow M \rightarrow \Gamma$. The horizontal broken lines denote the positions of Fermi levels for $x = 0.3, 0.4, 0.5$ and 0.6 from the bottom to the top. Insets denote the band structure in magnified scales around at $(\pi, 0)$ and a point between (π, π) and $(0, 0)$. Fermi-surface curves for (b) $x = 0.3$, (c) $x = 0.4$, (d) $x = 0.5$, and (e) $x = 0.6$.

and Γ points, but it is still under the band A at the X point. For $x = 0.6$, the Fermi level crosses not only the B band but also the A band near the X point.

The above characters appear in the change of the Fermi-surface structure, as shown in Figs. 1(b)-1(e). In Fig. 1(b), we depict the Fermi-surface curves for $x = 0.3$. A characteristic issue is that pocket-like disconnected Fermi-surface curves appear around at the X and Y points. We remark that these Fermi-surface curves originate from the B band and they do not cross the lines of $k_x = \pm k_y$. This issue will be important in the discussion of the gap function later. Another characteristic point is the shape of the Fermi-surface curves. We observe the disconnected Fermi-surface curves, which possess the projections extending to the direction to those of other Fermi-surface curves. For $x = 0.4$, we still observe pocket-like disconnected

Fermi-surface curves around at the X and Y points, as shown in Fig. 1(c). Note that the projections further extend to the directions to other Fermi-surface curves, but they do not touch.

When we further increase x , the projections eventually touch other Fermi-surface curves and the disconnected structure is dissolved, as observed in Fig. 1(d) for $x = 0.5$. Then, we observe a couple of large Fermi-surface curves with the centers at the Γ and M points. These two Fermi-surface curves originating from the B band are formed by the merge of the projections of pocket-like Fermi-surface curves in Fig. 1(c). We should pay attention to the existence of the Fermi-surface curves on the lines of $k_x = \pm k_y$. We also remark that the topological change of the Fermi-surface structure occurs around at $x = 0.45$, as already mentioned in Refs. [7] and [10].

Now we further increase the values of x . The Fermi-surface curves for $x = 0.6$ are shown in Fig. 1(e). Here we observe the large Fermi-surface curves around at the Γ and M points, although the shape is slightly deformed from those for $x = 0.5$ in Fig. 1(d). Note also that new pocket-like Fermi-surface curves appear around at the X and Y points. These curves originate from the A band, in sharp contrast to other Fermi-surface curves. We find that there occurs the topological change for the appearance of the Fermi-surface curve originating from the A band at $x = 0.52$, as already pointed out in Ref. [10].

2.3. Spin and orbital susceptibilities

In order to investigate superconductivity around the spin and/or orbital ordered phases [19, 20, 21, 22, 23, 24, 25, 26, 27], we calculate spin and orbital susceptibilities, $\hat{\chi}^s(\mathbf{q})$ and $\hat{\chi}^o(\mathbf{q})$, respectively. Here we follow the formulation and the notations in Ref. [20]. Within the RPA, spin and orbital susceptibilities are given in the 4×4 matrix form as

$$\hat{\chi}^s(\mathbf{q}) = [\hat{1} - \hat{U}^s \hat{\chi}(\mathbf{q})]^{-1} \hat{\chi}(\mathbf{q}), \quad (6)$$

and

$$\hat{\chi}^o(\mathbf{q}) = [\hat{1} + \hat{U}^o \hat{\chi}(\mathbf{q})]^{-1} \hat{\chi}(\mathbf{q}), \quad (7)$$

respectively. Here labels of row and column in the matrix appear in the order of 11, 22, 12, and 21, which are pairs of orbital indices 1 and 2. Note that $\hat{1}$ is the 4×4 unit matrix. The interaction matrices \hat{U}^s and \hat{U}^o are given by

$$\hat{U}^s = \begin{pmatrix} U & J & 0 & 0 \\ J & U & 0 & 0 \\ 0 & 0 & U' & J' \\ 0 & 0 & J' & U' \end{pmatrix}, \quad (8)$$

and

$$\hat{U}^o = \begin{pmatrix} U & 2U' - J & 0 & 0 \\ 2U' - J & U & 0 & 0 \\ 0 & 0 & 2J - U' & J' \\ 0 & 0 & J' & 2J - U' \end{pmatrix}, \quad (9)$$

respectively. Each matrix element of $\hat{\chi}(\mathbf{q})$ is defined by

$$\chi_{\mu\nu,\alpha\beta}(\mathbf{q}) = -T \sum_{\mathbf{k}, n} G_{\alpha\mu}^{(0)}(\mathbf{k} + \mathbf{q}, i\omega_n) G_{\nu\beta}^{(0)}(\mathbf{k}, i\omega_n), \quad (10)$$

where T is a temperature, $G_{\mu\nu}^{(0)}(\mathbf{k}, i\omega_n)$ is the non-interacting Green's function propagating between μ - and ν -orbitals, and $\omega_n = \pi T(2n + 1)$ with an integer n . The instabilities for the spin- and orbital-ordered phases are determined by the conditions of $\det[\hat{1} - \hat{U}^s \hat{\chi}(\mathbf{q})] = 0$ and $\det[\hat{1} + \hat{U}^o \hat{\chi}(\mathbf{q})] = 0$, respectively.

2.4. Gap equation

By using $\hat{\chi}^s(\mathbf{q})$ and $\hat{\chi}^o(\mathbf{q})$, we obtain the superconducting gap equation in a weak-coupling limit as

$$\Delta^\xi(\mathbf{k}) = \sum_{\mathbf{k}'} \hat{V}^\xi(\mathbf{k} - \mathbf{k}') \hat{\phi}(\mathbf{k}') \Delta^\xi(\mathbf{k}'), \quad (11)$$

where $\Delta^\xi(\mathbf{k}) = [\Delta_{11}^\xi(\mathbf{k}), \Delta_{22}^\xi(\mathbf{k}), \Delta_{12}^\xi(\mathbf{k}), \Delta_{21}^\xi(\mathbf{k})]^T$ is the gap function in the vector representation for singlet ($\xi = S$) or triplet ($\xi = T$) pairing state. The matrix elements of the singlet- and triplet-pairing potentials are, respectively, given by

$$V_{\alpha\beta,\mu\nu}^S(\mathbf{q}) = -\frac{3}{2} W_{\alpha\mu,\nu\beta}^s(\mathbf{q}) + \frac{1}{2} W_{\alpha\mu,\nu\beta}^o(\mathbf{q}) + U_{\alpha\mu,\nu\beta}^s, \quad (12)$$

$$V_{\alpha\beta,\mu\nu}^T(\mathbf{q}) = \frac{1}{2} W_{\alpha\mu,\nu\beta}^s(\mathbf{q}) + \frac{1}{2} W_{\alpha\mu,\nu\beta}^o(\mathbf{q}) - U_{\alpha\mu,\nu\beta}^s, \quad (13)$$

which are composed of spin and orbital susceptibilities as

$$\hat{W}^s(\mathbf{q}) = \hat{U}^s + \hat{U}^s \hat{\chi}^s(\mathbf{q}) \hat{U}^s, \quad (14)$$

$$\hat{W}^o(\mathbf{q}) = -\hat{U}^o + \hat{U}^o \hat{\chi}^o(\mathbf{q}) \hat{U}^o. \quad (15)$$

The element of the pair correlation function $\hat{\phi}(\mathbf{k})$ is given by

$$\phi_{\alpha\beta,\mu\nu}(\mathbf{k}) = T \sum_n G_{\alpha\mu}^{(0)}(\mathbf{k}, -i\omega_n) G_{\nu\beta}^{(0)}(-\mathbf{k}, i\omega_n). \quad (16)$$

We obtain T_c by solving the gap equation eq. (11). Note that T_c is defined as a temperature at which the positive maximum eigenvalue of the gap equation becomes unity. For the evaluation of the eigenvalue of eq. (11), we use the power method. The first Brillouin zone is divided into 64×64 meshes and we exploit the fast-Fourier-transformation algorithm, in order to accelerate the sum of large amount of momenta.

As for the values of Coulomb interactions, we note the relations of $U = U' + J + J'$ and $J = J'$, as mentioned above. Here we assume the value of J as $J = U/6$. Then, from the above relations, we obtain $U' = 2U/3$. In this paper, we fix the value of U as $U = 2$ eV. Note that the energy unit is set as eV in this paper. The bandwidth W of the present tight-binding band structure is $W = 4.5$ eV. Thus, the value of $U = 2$ is not so large in comparison with W .

3. Calculation Results

3.1. Phase diagram

Let us show our calculation results for the transition temperature T_c as a function of doping x in Fig. 2. First of all, we should note the magnitude of the vertical temperature axis. Since the energy unit is eV in the present calculations, the maximum value of T_c becomes about 600 K, if we simply use the present energy unit. Here we should pay attention to the fact

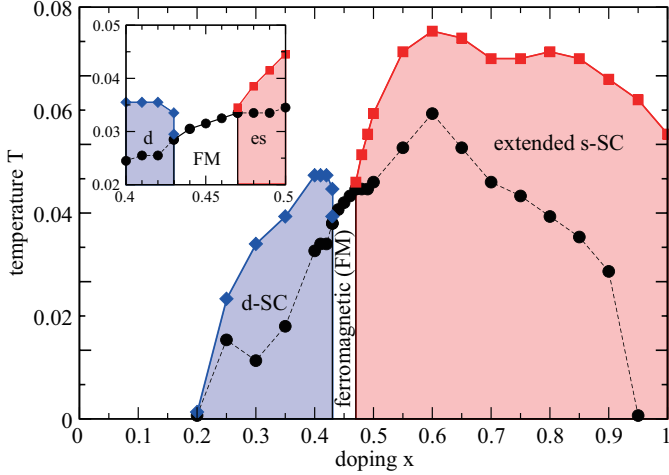


Figure 2: Phase diagram on the plane of doping x and temperature T . Solid black circles denote the magnetic instability temperature T_M , while solid red squares and blue diamonds indicate T_c for the extended s - and d -wave symmetries, respectively. Note that the solid curve denotes the phase boundary, but the broken curve does not. Inset shows the part of the phase diagram around at $x = 0.45$ in a magnified scale.

that we have not included at all the effects of the retardation of effective interactions and the quasi-particle life-time. If we correctly include the vertex corrections in addition to above strong-coupling effects, T_c is considered to be strongly suppressed. Thus, it is not necessary to consider seriously the magnitude of T_c in the present calculations. Rather we should pay our attention to the relative change of T_c by the doping x .

The lower curve denotes the magnetic instability temperature T_M determined from $\det[\hat{1} - \hat{U}^s \hat{\chi}(\mathbf{q})] = 0$. In the present calculations, when we decrease the temperature, the spin susceptibility always diverges prior to the orbital one and we do not consider the orbital susceptibility. Then, we solve the gap equation in the range of $T > T_M$ to consider the superconductivity induced by magnetic fluctuations in the vicinity of the magnetic instability temperature. Note that we cannot discuss the coexistence of magnetism and superconductivity in the present RPA.

In Fig. 2, we immediately notice that the superconducting phase in the weak-coupling limit appears in the wide range of the values of doping x and temperature T . Roughly speaking, the shape of the curve for T_c is similar to that for T_M . In particular, the position of the maximum T_c is exactly the same as that of T_M . We also point out that the superconducting phase is divided into two regions: The d -wave phase for $x < 0.45$ and the extended s -wave phase for $x > 0.45$. The figure around at $x \approx 0.45$ in a magnified scale is shown in the inset of Fig. 2. In the present calculations, in a very narrow region around at $x = 0.45$, T_c is suppressed. Instead, we find the ferromagnetic (FM) phase in this region, since the ordering vector is found to be $\mathbf{q} = (0, 0)$ in this region. Near $x = 1.0$, T_M becomes zero since both U and the density of states at the Fermi level are small in this case, but T_c keeps a large value, although it is smaller than the peak value at $x = 0.6$. For $x < 0.2$, we cannot obtain both magnetic and superconducting phases in the RPA for the system with small electron densities.

We note that there is not significant structure in T_c around at $x = 0.52$, at which the Fermi-surface topology is changed due to the appearance of the Fermi-surface curves originating from the A band. We deduce that the effect of the pairing in the A band will not be so significant, since the superconductivity occurs mainly in the B band. In the d -wave phase, except for the narrow region around at $x = 0.45$, T_c is increased with the increase of x . On the other hand, in the extended s -wave phase, T_c takes a broad peak at $x = 0.6$. Note that the magnetic instability curve also exhibits the peak at $x = 0.6$, but the peak structure is rather sharp.

Let us now compare our phase diagram with experimental results. First we briefly review the experimental facts. For $\text{LaO}_{1-x}\text{F}_x\text{BiS}_2$, the doping dependence of T_c seems to be sensitive to the way of sample synthesis [4, 28, 29]. For as-grown samples, T_c is increased between $x = 0.2$ and 0.5 , whereas it becomes almost constant between $x = 0.5$ and 0.7 . For annealed samples under high pressures, T_c is totally increased and it becomes maximum at $x = 0.5$. In addition, T_c seems to be abruptly increased between $x = 0.4$ and 0.5 .

For $\text{NdO}_{1-x}\text{F}_x\text{BiS}_2$, we have found weak doping dependence of T_c [30]. It has been found that superconductivity appears in the region of $0.1 \leq x \leq 0.7$ and T_c becomes maximum at $x = 0.4$, although the change of T_c by doping x is not so significant in comparison with $\text{LaO}_{1-x}\text{F}_x\text{BiS}_2$.

In our phase diagram, the maximum T_c is found at $x = 0.6$, which is deviated from $x = 0.5$ for $\text{LaO}_{1-x}\text{F}_x\text{BiS}_2$ and $x = 0.4$ for $\text{NdO}_{1-x}\text{F}_x\text{BiS}_2$. This deviation may be explained by the strong coupling calculation or by the further inclusion of electron-phonon interaction. These points will be discussed in future. We remark a point that the nominal value of x may be deviated from the amount of electron doping in BiS_2 layer [31]. We should pay due attention to this point in the comparison with experiments. It is another future task.

Around at $x = 0.45$, the Fermi-surface topology is changed and the singlet superconductivity has been found to be suppressed. As expected from the FM phase around at $x = 0.45$, the eigenvalue of the triplet pair has been found to be larger than that of the singlet one in this region, although it has not reached the unity in the present calculation. The tendency of the triplet pair may be also related to the previous work in Ref. [9]. When we include the strong-coupling effects and the vertex corrections in the evaluation of the normal and anomalous self-energies, the triplet superconductivity may occur around at $x = 0.45$. This is one of interesting future issues.

3.2. Susceptibilities and Fermi-surface curves

In order to grasp the kind of the magnetic fluctuations for the pair formation, we show the spin susceptibilities in the RPA for $x = 0.3, 0.4, 0.5$, and 0.6 in Figs. 3 and 4 along the path of $\mathbf{q} = (0, 0) \rightarrow (\pi, 0) \rightarrow (\pi, \pi) \rightarrow (0, 0)$. Since we have found that orbital susceptibilities are totally suppressed and they do not show any significant structures in comparison with spin ones in the present calculations, we show only spin susceptibilities in this paper.

In Figs. 3(a) and 3(b), we show the spin susceptibilities, respectively, for $x = 0.3$ and 0.4 . Note that the temperatures are

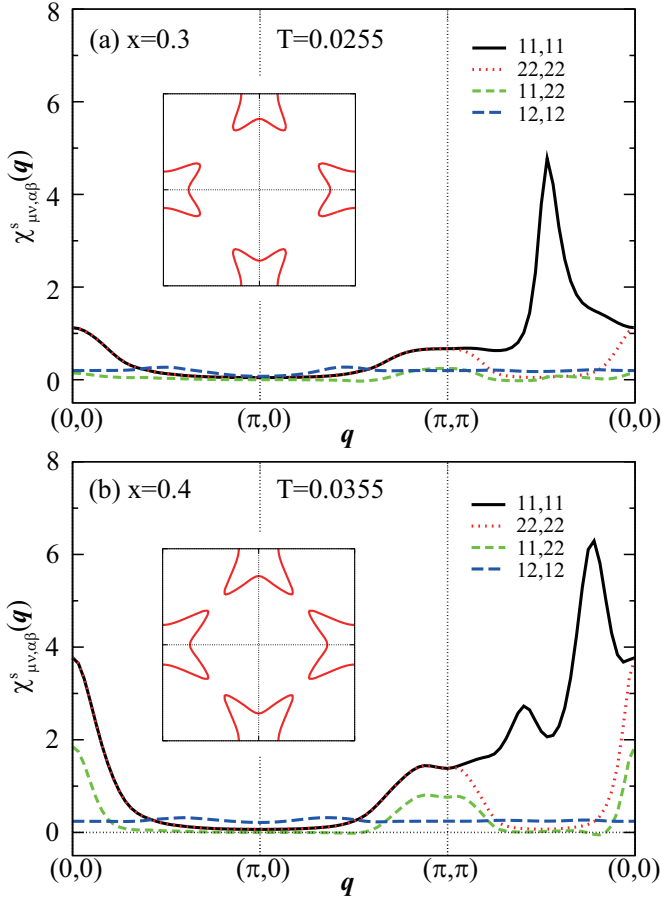


Figure 3: Spin susceptibilities in the RPA for (a) $x = 0.3$ and (b) $x = 0.4$. Inset in each panel denotes the Fermi-surface curve.

set as T_c , which are $T_c = 0.0255$ for $x = 0.3$ and $T_c = 0.0355$ for $x = 0.4$. We find the enhanced spin fluctuations of $\mathbf{q}=(q, q)$, which will contribute to the Cooper-pair formation for superconductivity. The value of q becomes small when x is increased from 0.3 to 0.4. For $x = 0.4$, we observe another small peak for large q . Note that the FM fluctuations also grow for $x = 0.4$ in comparison with that for $x = 0.3$. The FM fluctuations tend to be significant, when x approaches 0.45, as expected from the existence of the FM phase around at $x = 0.45$.

In Fig. 4(a) and 4(b), we exhibit the spin susceptibilities in the RPA for $x = 0.5$ and 0.6 , respectively. Note that the temperature is set as $T = 0.0445$ and 0.0565 , which are equal to T_c at $x = 0.5$ and 0.6 , respectively. In the bare susceptibility, the maximum peak appears at $\mathbf{q} = (q, 0)$ with small q . This peak structure is due to the nesting of a couple of large Fermi-surface curves with the centers at the Γ and M points [7]. In fact, for $x = 0.5$, the peak at $\mathbf{q} = (q, 0)$ is larger than other peak values in the RPA spin susceptibility, although anti-ferromagnetic (AF) spin fluctuations also grow. For $x = 0.6$, the peak at $\mathbf{q} = (q, 0)$ is still significant, but we observe a clear peak at $\mathbf{q} = (\pi, \pi)$, suggesting AF spin fluctuations. We deduce that the evolution of the AF spin fluctuations is closely related to the elevation of T_c from $x = 0.5$ to $x = 0.6$.

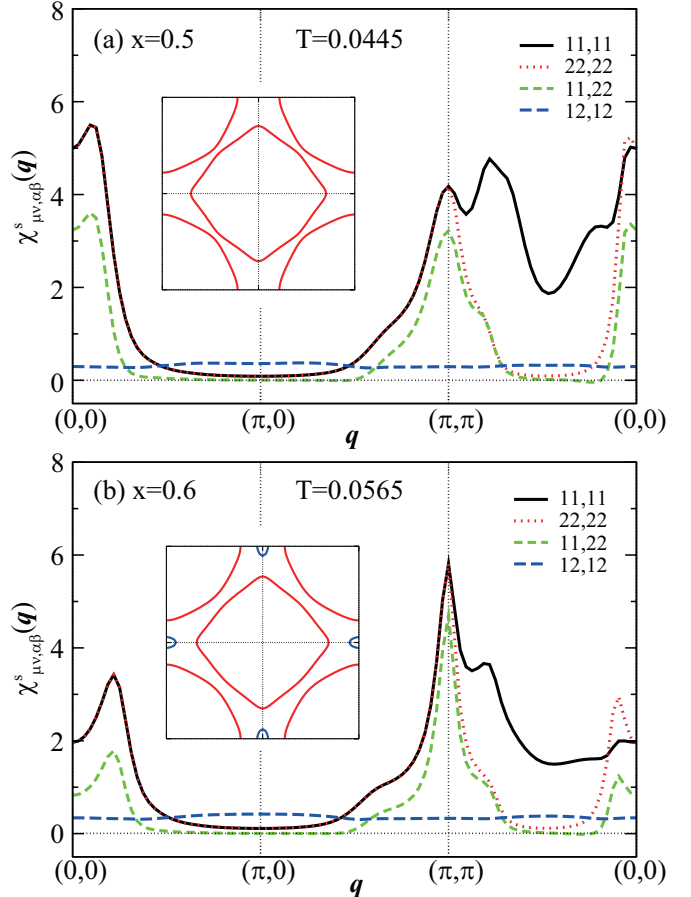


Figure 4: Spin susceptibilities in the RPA for (a) $x = 0.5$ and (b) $x = 0.6$. Inset in each panel denotes the Fermi-surface curve.

3.3. Gap functions and Fermi-surface curves

Now we show the results of the gap function for the Cooper pair from the same band, $\Delta_A(\mathbf{k})$ and $\Delta_B(\mathbf{k})$, which are obtained by the appropriate linear combinations of $\Delta_{11}^S(\mathbf{k})$, $\Delta_{22}^S(\mathbf{k})$, $\Delta_{12}^S(\mathbf{k})$, and $\Delta_{21}^S(\mathbf{k})$. There exist the components of the Cooper pairs formed by different band electrons, but we do not show them here, since their magnitudes are small in comparison with those of the same band. Note also that only the singlet pair has been stabilized, although we have investigated both singlet and triplet channels. Thus, we show here the results for singlet gap functions.

In Figs. 5, we exhibit $\Delta_A(\mathbf{k})$ and $\Delta_B(\mathbf{k})$ for $x = 0.3$ and $T = 0.0255$ by using the color gradation to visualize the momentum dependence at a glance. First we notice that the gap functions $\Delta_A(\mathbf{k})$ and $\Delta_B(\mathbf{k})$ possess the d -wave symmetry, which is characterized by the sign change of the gap for the interchange of k_x and k_y . In this doping, there is no Fermi-surface curve from the band A, but we observe the significant amplitude around at the X and Y points, since the band A is near the Fermi level on these points, as shown in Fig. 1(a).

As for the gap function on the band B in Fig. 5(b), we observe that the nodes of the d -wave, $k_x = \pm k_y$, are running between the pocket-like Fermi-surface curves. Namely, the nodes do not cross the Fermi-surface curves. However, we find the

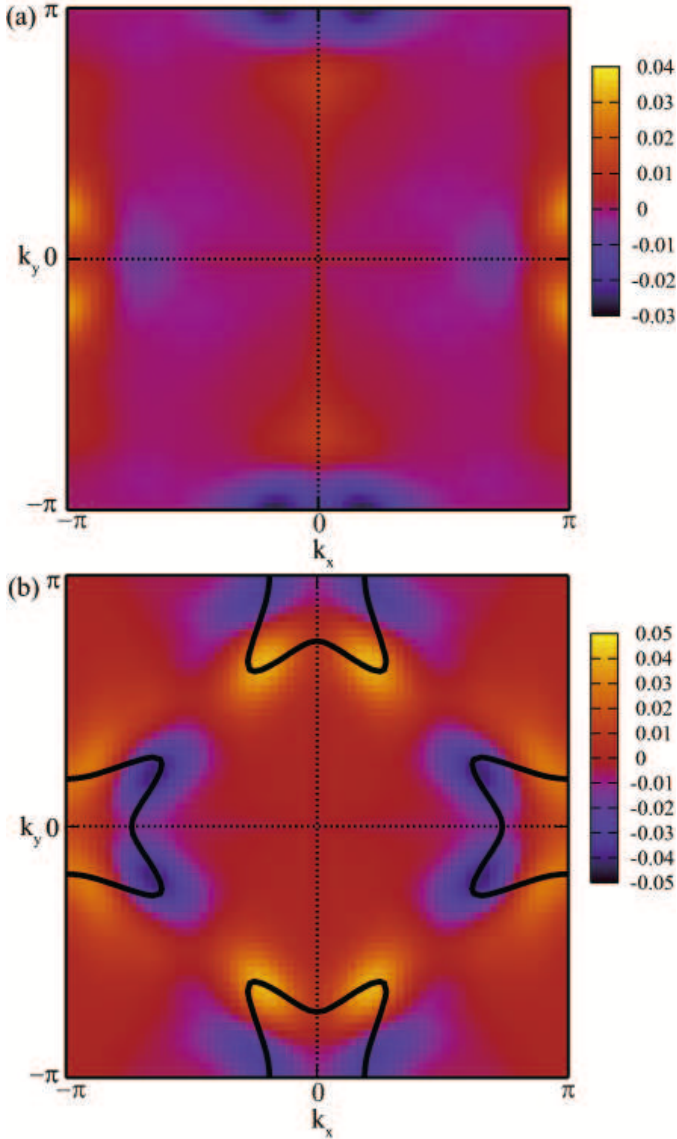


Figure 5: (a) $\Delta_A(\mathbf{k})$ and (b) $\Delta_B(\mathbf{k})$ for $x = 0.3$. We show the Fermi-surface curves in the figure.

sign change of the gap at the heads of the projections for the interchange of k_x and k_y . Note that the signs of the gap functions near the X and Y points are also different from those at the heads of the projections of the Fermi-surface curves. For $x = 0.3$, we can observe other node lines connecting the points of $(-\pi, 0)$, $(0, -\pi)$, $(\pi, 0)$, and $(0, \pi)$. These node structures seem to be consistent with those proposed by Usui *et al.* [5].

In Figs. 6, we show $\Delta_A(\mathbf{k})$ and $\Delta_B(\mathbf{k})$ for $x = 0.4$ and $T = 0.0355$. The d -wave node structure is similar to that in Figs. 5, but we do not observe the node lines connecting four points of $(-\pi, 0)$, $(0, -\pi)$, $(\pi, 0)$, and $(0, \pi)$ in Fig. 6(b). Rather the gap function $\Delta_B(\mathbf{k})$ changes its sign for three times on the straight line from $(\pi, 0)$ to $(0, \pi)$. The gap function $\Delta_B(\mathbf{k})$ seems to include the components of the symmetry higher than the d -wave, for instance, g -wave [11].

The gap structure on the Fermi-surface curves around at the

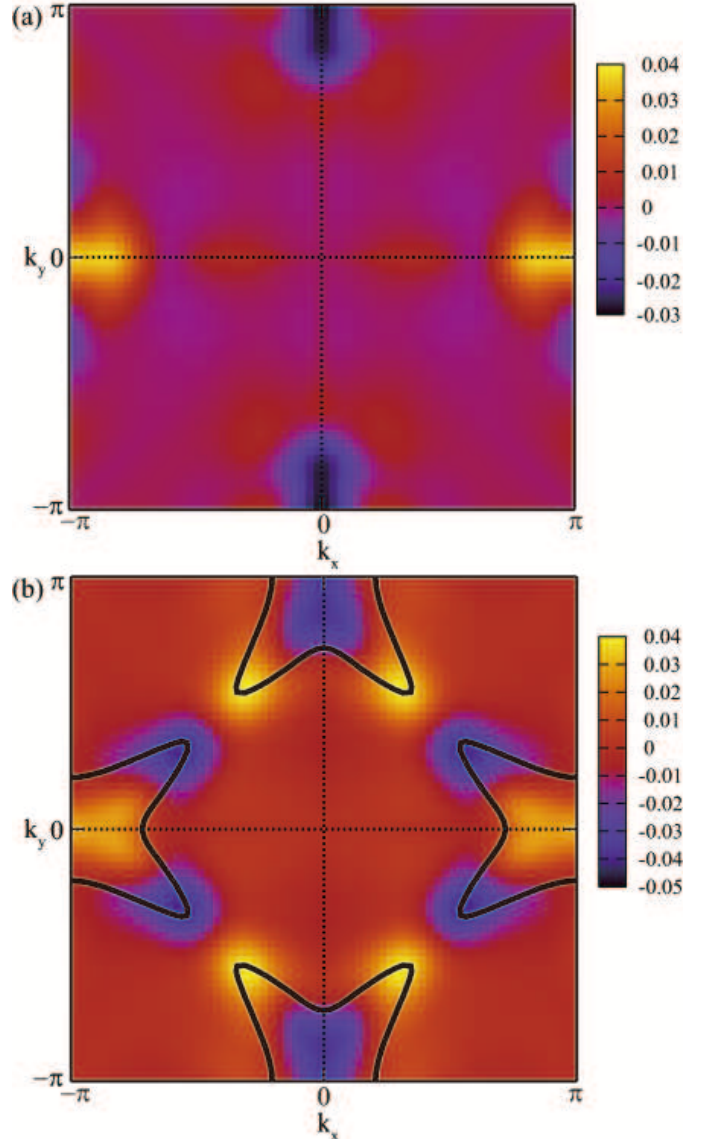


Figure 6: (a) $\Delta_A(\mathbf{k})$ and (b) $\Delta_B(\mathbf{k})$ for $x = 0.4$. We show the Fermi-surface curves in the figure.

X and Y points has been investigated in $\text{NdO}_{0.71}\text{F}_{0.29}\text{BiS}_2$ with the use of an angle-resolved photoemission spectroscopy [32]. The large anisotropy has been observed and the gap size on the point at which the Fermi-surface curve crosses the line from $(\pi, 0)$ to (π, π) is smaller than that on the point at which the Fermi-surface curve crosses the line from $(\pi, 0)$ to $(0, \pi)$. The tendency seems to agree with the present results, but in order to conclude the existence of the node, it is necessary to perform further experimental and theoretical investigations.

Next we consider the gap functions for $x > 0.45$. In Fig. 7(a) and 8(a), we depict the gap functions $\Delta_A(\mathbf{k})$ for $x = 0.5$ and 0.6 , respectively. Note that for $x = 0.6$, we also depict the Fermi-surface curve originating from the A band around at the X and Y points. In both cases, we do not find the nodes characteristic to the d -wave in the gap function. The node lines satisfying $\cos k_x + \cos k_y = 0$ seem to be observed, but it is difficult to

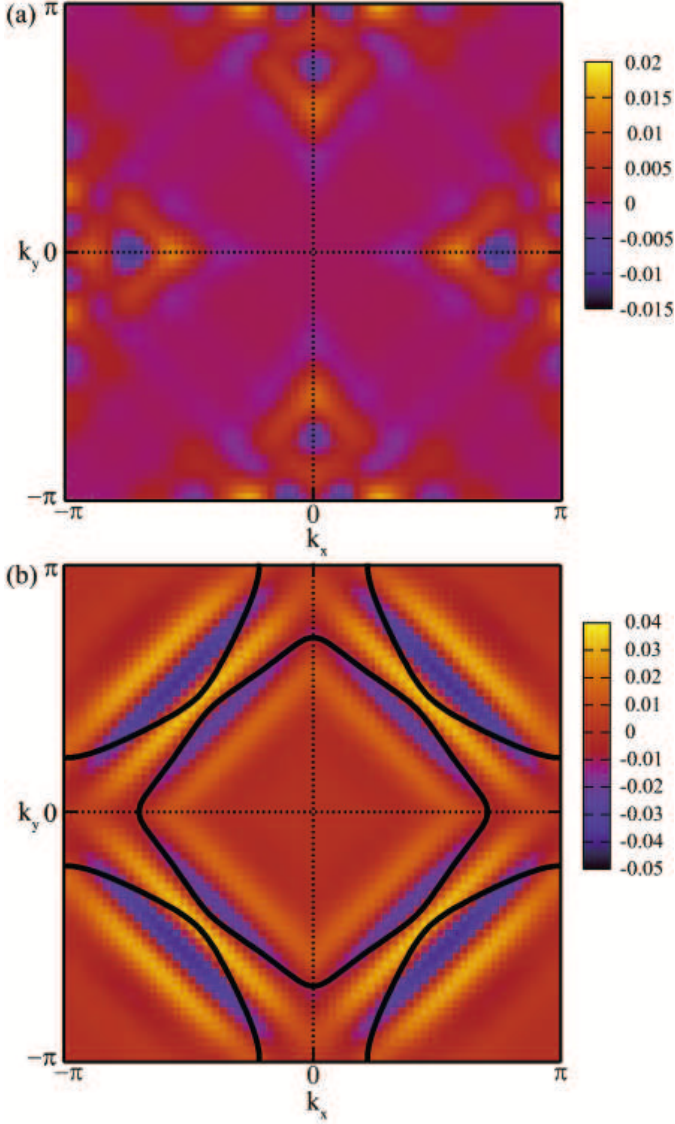


Figure 7: (a) $\Delta_A(\mathbf{k})$ and (b) $\Delta_B(\mathbf{k})$ for $x = 0.5$. We show the Fermi-surface curves in the figure.

confirm them only from this figure.

In Figs. 7(b) and 8(b), we show the gap functions $\Delta_B(\mathbf{k})$ and the large Fermi-surface curves for $x = 0.5$ and 0.6 , respectively. Also in these cases, the nodes characteristic to the d -wave gap cannot be observed. Note that the structures in the gap functions are quite similar to each other irrespective of the difference in x . We find several numbers of node lines expressed as $k_y = \pm k_x + C$, where C indicates an appropriate constant. When we change \mathbf{k} in $\Delta_B(\mathbf{k})$ along the line from the Γ to M points, the gap changes its sign for several times.

We remark that the Fermi-surface structure becomes different between $x = 0.5$ and 0.6 . In particular, the curvature of the Fermi-surface curves for $x = 0.5$ is larger than that for $x = 0.6$. Since the nodes are well expressed by the lines of $k_y = \pm k_x + C$, the nodes of the gap easily appear on the Fermi-surface curves with large curvature for $x = 0.5$ in comparison with those for $x = 0.6$. From Figs. 7 and 8, there seems to occur a peculiar

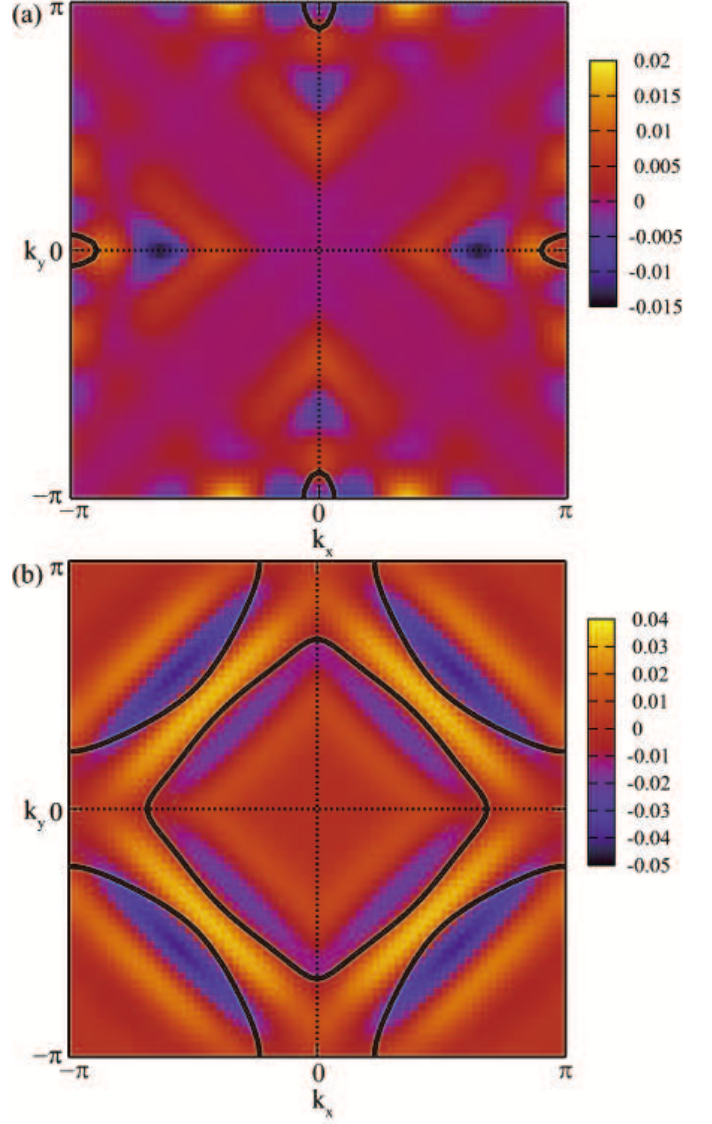


Figure 8: (a) $\Delta_A(\mathbf{k})$ and (b) $\Delta_B(\mathbf{k})$ for $x = 0.6$. We show the Fermi-surface curves in the figure.

possibility that the Fermi-surface curves tend to avoid the extended s -wave gap functions with large amplitude. This issue should be investigated in detail in future.

4. Discussion and Summary

In this paper, we have solved the gap equation to obtain the superconducting transition temperature T_c and the gap function within the RPA on the basis of the two-band Hubbard model for BiS_2 -based layered compounds. When the topology of the Fermi-surface curves of the B band drastically changes around at $x = 0.45$, we have observed the change of the symmetry of the gap function. For $x < 0.45$, we have obtained the d -wave gap with the nodes on the lines of $k_x = \pm k_y$, which do not cross the Fermi-surface curves with the pocket-like disconnected shapes around at the X and Y points. On the other hand,

for $x > 0.45$, we have found the extended s -wave gap. An interesting issue is that the amplitude of the gap seems to be small or zero on the Fermi-surface curves.

The effect of the nodes on the temperature dependence of physical quantities is quite interesting for the comparison with experimental result. In particular, it has been reported that the temperature dependence of the penetration depth indicates the s - or extended s -wave gap both for $x = 0.3$ and 0.5 in $\text{NdO}_{1-x}\text{F}_x\text{BiS}_2$ [18]. In the present results, we have found the d -wave gap for $x < 0.45$, but the main nodes of d -wave gap do not cross the Fermi-surface curve. For $x > 0.45$, we have obtained the extended s -wave gap. However, for both gap functions, we have found the node structure on the Fermi-surface curves depending on the doping x . It is interesting to clarify the temperature dependence of the penetration depth for the gap function with the present node structure. This is one of future problems.

In the present calculations, we have considered only the Coulomb interactions. However, around at the Lifshitz transition point at which the Fermi-surface topology is abruptly changed, the coupling between the charge fluctuations and lattice vibrations seems to be important. In fact, the role of phonons in BiS_2 -based materials has been discussed intensively [12, 13, 14]. We believe that it is necessary to include electron-phonon interaction to the present two-orbital Hubbard model. It is another future problem.

In summary, we have discussed the gap symmetry of BiS_2 -based layered superconductors by analyzing the two-orbital Hubbard mode within the RPA. For $x < 0.45$, we have found the d -wave gap on the pocket-like disconnected Fermi-surface curves, whereas for $x > 0.45$, the extended s -wave gap has been found on a couple of large Fermi-surface curves with the centers at the Γ and M points. The symmetry change in the gap function is believed to be induced by the topological change in the Fermi-surface structure.

Acknowledgement

The authors thank Y. Aoki, K. Hattori, R. Higashinaka, K. Kubo, T. D. Matsuda, Y. Mizuguchi, Y. Ota, and K. Ueda for useful discussions on BiS_2 -based layered superconductors. The computation in this work has been partly done using the facilities of the Supercomputer Center of Institute for Solid State Physics, University of Tokyo.

- [1] Y. Mizuguchi, H. Fujihisa, Y. Gotoh, K. Suzuki, H. Usui, K. Kuroki, S. Demura, Y. Takano, H. Izawa, and O. Miura, Phys. Rev. B **86**, 220510(R) (2012).
- [2] Y. Mizuguchi, S. Demura, K. Deguchi, Y. Takano, H. Fujihisa, Y. Gotoh, H. Izawa, and O. Miura, J. Phys. Soc. Jpn. **81**, 114725 (2012)
- [3] Y. Mizuguchi, J. Phys. Chem. Solid **84**, 34 (2015).
- [4] Y. Mizuguchi, T. Hiroi, J. Kajitani, H. Takatsu, H. Kadowaki, and O. Miura, J. Phys. Soc. Jpn. **83**, 053704 (2014).
- [5] H. Usui, K. Suzuki, and K. Kuroki, Phys. Rev. B **86**, 220501(R) (2012).
- [6] K. Suzuki, H. Usui, and K. Kuroki, Phys. Procedia **45**, 21 (2013).
- [7] G. Martins, A. Moreo, and E. Dagotto, Phys. Rev. B **87**, 081102(R) (2013).
- [8] T. Zhou and Z. D. Wang, J. Supercond. Nov. Magn. **26**, 2735 (2013).
- [9] Y. Yang, W. S. Wang, Y. Y. Xiang, Z. Z. Li, and Q. H. Wang, Phys. Rev. B **88**, 094519 (2013).
- [10] Y. Liang, X. Wu, W.-F. Tsai, and J. Hu, Front. of Phys. **9**, 194 (2014).
- [11] X. Wu, J. Yuan, Y. Liang, H. Fan, and J. Hu, Europhys. Lett. **108**, 27006 (2014).
- [12] T. Yildirim, Phys. Rev. B **87**, 020506(R) (2013).
- [13] X. Wan, H.-C. Ding, S. Y. Savrasov, and C.-G. Duan, Phys. Rev. B **87**, 115124 (2013).
- [14] B. Li, Z. W. Xing, and G. Q. Huang, Europhys. Lett. **101**, 47002 (2013).
- [15] Y. Gao, T. Zhou, H. Huang, P. Tong, and Q.-H. Wang, Phys. Rev. B **90**, 054518 (2014).
- [16] P. Shruti Srivastava and S. Patnaik, J. Phys.: Condens. Matter **25**, 312202 (2013).
- [17] G. Lamura, T. Shiroka, P. Bonfa, S. Sanna, R. DeRenzi, C. Baines, H. Luetkens, J. Kajitani, Y. Mizuguchi, O. Miura, K. Deguchi, S. Demura, Y. Takano, and M. Putti, Phys. Rev. B **88**, 180509 (2013).
- [18] L. Jiao, Z. Weng, J. Liu, J. Zhang, G. Pang, C. Guo, F. Gao, X. Zhu, H.-H. Wen, and H. Q. Yuan, J. Phys.: Condens. Matter **27**, 225701 (2015).
- [19] T. Takimoto, Phys. Rev. B **62**, R14641 (2000).
- [20] T. Takimoto, T. Hotta, T. Maehira, and K. Ueda, J. Phys.: Condens. Matter **14**, L369 (2002).
- [21] T. Takimoto, T. Hotta, and K. Ueda, Phys. Rev. B **69**, 104504 (2004).
- [22] M. Mochizuki, Y. Yanase, and M. Ogata, Phys. Rev. Lett. **94**, 147005 (2005).
- [23] Y. Yanase, M. Mochizuki, and M. Ogata, J. Phys. Soc. Jpn. **74**, 430 (2005).
- [24] M. Mochizuki, Y. Yanase, and M. Ogata, J. Phys. Soc. Jpn. **74**, 1670 (2005).
- [25] K. Yada and H. Kontani, J. Phys. Soc. Jpn. **74**, 2161 (2005).
- [26] K. Kubo and T. Hotta, J. Phys. Soc. Jpn. **75**, 083702 (2006).
- [27] K. Kubo, Phys. Rev. B **75**, 224509 (2007).
- [28] K. Deguchi, Y. Mizuguchi, S. Demura, H. Hara, T. Watanabe, S. J. Denholme, M. Fujioka, H. Okazaki, T. Ozaki, H. Takeya, T. Yamaguchi, O. Miura, and Y. Takano, Europhys. Lett. **101**, 17004 (2013).
- [29] R. Higashinaka, R. Miyazaki, Y. Mizuguchi, O. Miura, and Y. Aoki, J. Phys. Soc. Jpn. **83**, 75004 (2014).
- [30] S. Demura, Y. Mizuguchi, K. Deguchi, H. Okazaki, H. Hara, T. Watanabe, S. J. Denholme, M. Fujioka, T. Ozaki, H. Fujihisa, Y. Gotoh, O. Miura, T. Yamaguchi, H. Takeya, and Y. Takano, J. Phys. Soc. Jpn. **82**, 033708 (2013).
- [31] Y. Mizuguchi, private communications.
- [32] Y. Ota, K. Okazaki, T. Yamamoto, H. Yamamoto, S. Watanabe, C.-T. Chen, M. Nagao, S. Watauchi, I. Tanaka, Y. Takano, and S. Shin, unpublished.